



Title	Thickness Optimization toward High-Performance Bottom-Gated Transparent Tin Dioxide Thin-Film Transistors
Author(s)	Liang, Dou-Dou; Chen, Binjie; Cho, Hai Jun; Ohta, Hiromichi
Citation	ACS Applied Electronic Materials, 2(10), 3454-3458 https://doi.org/10.1021/acsaelm.0c00711
Issue Date	2020-10-27
Doc URL	http://hdl.handle.net/2115/83072
Rights	This document is the Accepted Manuscript version of a Published Work that appeared in final form in ACS Applied Electronic Materials, copyright © American Chemical Society after peer review and technical editing by the publisher. To access the final edited and published work see https://pubs.acs.org/doi/10.1021/acsaelm.0c00711 .
Type	article (author version)
File Information	D. Liang et al..pdf



[Instructions for use](#)

Thickness Optimization toward High-Performance Bottom-Gated Transparent Tin Dioxide Thin-Film Transistor

Dou-dou Liang,* Binjie Chen, Hai Jun Cho, and Hiromichi Ohta*

Keywords

effective channel thickness, amorphous SnO₂, transparent thin-film transistor, electric field thermopower modulation, depletion layer, bottom gated

ABSTRACT: Nowadays, transparent amorphous oxide semiconductor (TAOS) based transparent thin-film transistors (TTFTs) are utilized as the backplane of organic light emitting diode (OLED) displays. Among many TAOSs examined to date, amorphous (a-) SnO₂ is one of the most promising candidates owing to its environmental compatibility *e.g.* Indium-free. Although several SnO₂-based TFTs have been demonstrated so far, the reported characteristics are ambiguous *e.g.* extremely high electron mobility ($>100 \text{ cm}^2 \text{ V}^{-1} \text{ s}^{-1}$) and behaviors far different from those of currently used a-InGaZnO₄ based TFTs. Here we show high-performance bottom-gated a-SnO₂ based TTFTs. First, we systematically investigated the electron transport properties and the bandgap of SnO₂ films with various thicknesses. Then, we optimized the SnO₂

thickness by analyzing the operation mechanism of the TTFTs using electric field thermopower modulation technique. We found the optimal SnO₂ thickness is 4.2 nm for high performance TTFTs; highest on-to-off current ratio ($\sim 10^5$) and high mobility ($\sim 20 \text{ cm}^2 \text{ V}^{-1} \text{ s}^{-1}$). The present results would be essential to develop a-SnO₂-based TTFTs in commercial applications.

INTRODUCTION

Transparent amorphous oxide semiconductors (TAOSs) are an excellent candidate for transparent thin-film transistors (TTFTs) that have made an impressive progress particularly in display applications such as transparent organic light-emitting diode (OLED) display technologies. To realize efficient current modulation, TTFTs with high electron mobility is required for pixel-driving circuits. Currently, amorphous (a-) InGaZnO₄ is widely applied as the TAOS¹⁻⁴ for the TFT channel of commercially available OLED displays since its field-effect mobility (μ_{FE}) of a-InGaZnO₄ ($\sim 10 \text{ cm}^2 \text{ V}^{-1} \text{ s}^{-1}$) is two orders of magnitude higher than that of previously used a-Si.

Nevertheless, indium is not an ideal candidate for commercial applications due to its low abundance in the earth's crust. In this regard, amorphous (a-) SnO₂ is an excellent alternative material as its composition is much more abundant compared to those of a-

InGaZnO₄. However, although several reports on the fabrication and characterization of SnO₂-based TFTs have been published so far, the TFT characteristics are far different from that of a-InGaZnO₄: *e.g.* extremely high electron mobility ($>100 \text{ cm}^2 \text{ V}^{-1} \text{ s}^{-1}$)⁵⁻⁸ and large dependence on the channel thickness. However, the mechanism of the TFT operation of such strange SnO₂-based TFTs has not been explained thus far due to the lack of systematic study on SnO₂ thin films.

In order to address this issue, recently, we analyzed the effective channel thickness of a-SnO₂-based TFT with the bottom-gate top-contact electrode configuration as schematically shown in Fig. 1(a).⁹ We found that carrier electrons at ~2.5-nm-thick SnO₂ top surface were depleted due to gas (oxygen) adsorption and carrier electrons at ~1.7-nm-thick effective channel were modulated by the electric field application. However, the thickness of SnO₂ has not been optimized to obtain high performance TFTs showing large on-to-off current ratio and field effect mobility.

Here we show the optimization of SnO₂ film thickness for TFTs. We systematically investigated the electron transport properties and the bandgap of SnO₂ films with various thicknesses. Then, we optimized the SnO₂ thickness by analyzing the operation mechanism of the TFTs using electric field thermopower modulation technique. As a

result, TTFT based on the 4.2-nm-thick SnO₂ film exhibited excellent characteristics; highest on-to-off current ratio ($\sim 10^5$) and high mobility ($\sim 20 \text{ cm}^2 \text{ V}^{-1} \text{ s}^{-1}$). The present results would be essential to develop a-SnO₂-based TTFTs in commercial applications.

RESULTS AND DISCUSSION

Optoelectronic Properties of SnO₂ Films with Various Thicknesses

We fabricated SnO₂ films with various thicknesses (3.2 – 41.6 nm) on SiO₂ glass substrates. The thicknesses were calculated from the Kiessig fringes measured by X-ray reflectivity (XRR) [Fig. 2(a)]. Figure 2(b) shows the glancing angle (0.5°) incidence X-ray diffraction (GIXRD) patterns of the SnO₂ films. Intense diffraction peaks of rutile structured SnO₂ are seen in the GIXRD patterns of 41.6 and 32.5 nm films. The peaks became broad and weak with decreasing thickness. When the thickness is thinner than 6 nm, diffraction peak disappeared, and halos were detected, indicating that the films were amorphous. From the crystallite sizes [inset of Fig. 2(b)], which were calculated from the diffraction peak width of 211 using Scherrer equation, we found that there is a threshold thickness (~ 8 nm) separating amorphous and crystalline phases of SnO₂.

Next, we investigated the optical band gap ($E_{g \text{ opt}}$) of the SnO₂ films [Figs. 3(a) and 3(b)], which was obtained from the x intercept of $(\alpha h\nu)^2 - h\nu$ plot (Tauc plot). In case of

17.4-nm-thick SnO₂ film, the $E_{g \text{ opt}}$ was 3.60 eV [Fig. 3(a)], consistent with bulk SnO₂.¹⁰

Figure 3(b) shows change in the $E_{g \text{ opt}}$ as a function of film thickness. The $E_{g \text{ opt}}$ dramatically increases with decreasing thickness when the thickness is thinner than 10 nm, whereas thicker films (>18 nm) show bulk-like $E_{g \text{ opt}}$. This is attributed to the quantum size effect, which can be expressed as¹¹

$$E_{g \text{ opt}} = 3.6 + \frac{h^2}{2L^2} \left(\frac{1}{m_e} + \frac{1}{m_h} \right)$$

where h is the Planck's constant, m_e and m_h are the effective masses of the electron and hole in the semiconductor ($m_e = 0.25 m_0$ ¹², $m_h = 0.47 m_0$ ⁹ of SnO₂), respectively, and L is the thickness of the SnO₂ thin films. The calculated $E_{g \text{ opt}}$ (solid line) clearly reproduces the observed $E_{g \text{ opt}}$ (circles). This demonstrates that reducing the thickness of amorphous SnO₂ films results in a dramatic widening of the $E_{g \text{ opt}}$ due to the quantum size effect.

Next, we investigated the electron transport properties of the SnO₂ thin films at room temperature (RT) [Figs 4(a)–4(d)]. It should be noted that the amorphous films showed opposite tendencies to the polycrystalline films. The electrical resistivity (ρ) decreased with decreasing thickness when the thickness is thicker than ~8 nm (polycrystalline), whereas it increased with decreasing thickness when the thickness is thinner than ~8 nm (amorphous) [Fig. 4(a)]. These tendencies were supported by the Hall mobility

(μ_{Hall}) [Fig. 4(b)], carrier concentration (n) [Fig. 4(c)], and thermopower ($-S$) [Fig. 4(d)]. The n tends to increase with decreasing the crystallite size [Fig. 4(c)]. Since SnO_2 is an n-type oxide semiconductor, the majority carrier is electron, which comes from the nonstoichiometric $\text{SnO}_{2-\delta}$. In the case of polycrystalline, grain boundaries serve as unintentional donor defects by annihilating or trapping charge carriers. Such examples include for native donor defects such as oxygen vacancy, which tend to aggregate at grain boundaries.¹³⁻¹⁴ Hence, as the grain boundary fraction increase, the n gradually increases. However, when the thickness is thinner than ~ 8 nm, the conduction band minimum (CBM) increases due to quantum size effect as explained previously [Fig. 3(b)]. Therefore, the n decreased with decreasing thickness in the amorphous phase. S values reflect the tendency of n [Fig. 4(d)]. The μ_{Hall} gradually increased with decreasing thickness [Fig. 4(b)] and reached $\sim 15 \text{ cm}^2 \text{ V}^{-1} \text{ s}^{-1}$ when the thickness was ~ 4 nm.

In order to clarify the thickness dependence of μ_{Hall} , we measured $\rho-T$ curves of the SnO_2 films from 300 to 30 K [Fig. 4(e)]. The ρ for the entire SnO_2 films increased with decreasing temperature, indicating a semiconducting behavior. We calculated the activation energy of the electrical conductivity (E_a) using the Arrhenius plots as shown in Fig. 4(f). In the polycrystalline region, the E_a increases with decreasing thickness,

most likely due to the reduction of boundary scattering of carrier electrons at grain boundaries. In case of amorphous region, the E_a is small as compared to the polycrystalline due to the absence of boundary scattering. The 3.2-nm-thick SnO₂ film showed larger E_a , most likely due to higher CBM energy. From these results, we concluded that the a-SnO₂ thin films with a thickness between 4–6 nm shows ideal electron transport properties as the TFT channel.

Thickness Optimization of Amorphous SnO₂ Film for Transistors

We fabricated several TTFTs using a-SnO₂ films with various thicknesses (4.2 nm, 4.5 nm, 5.2 nm, and 6.2 nm). Figures 5(a)–5(d) show the transfer (I_d – V_g) characteristics of the a-SnO₂ TTFTs. The on-to-off current ratio of the 6.2-nm-thick SnO₂ TTFT was only 2.6, due to large sheet carrier concentration [$n_s = C_i \cdot (V_g - V_{th}) \cdot e^{-1}$ where C_i is the capacitance per unit area ($C_i \sim 110 \text{ nF cm}^{-2}$)] (Fig. S2). The threshold gate voltage (V_{th}) was -58.7 V (Fig. S1). The on-to-off current ratio and V_{th} increased with decreasing the SnO₂ film thickness. The 4.2-nm-thick SnO₂ TTFT showed largest on-to-off current ratio of $\sim 10^5$. The field effect mobility (μ_{FE}) (Fig. S3), calculated from $\mu_{FE} = g_m \cdot [(W/L) \cdot C_i \cdot V_d]^{-1}$ (where g_m is the transconductance $\partial I_d / \partial V_g$), was $\sim 20 \text{ cm}^2 \text{ V}^{-1} \text{ s}^{-1}$ in all a-SnO₂ TTFTs.

Then, we measured the S during the transfer characteristics measurements (electric field thermopower modulation). Figures 5(e)–5(f) show relationship between the $-S$ and the V_g . The S values were negative, indicating that the SnO_2 film is n-type semiconductor. The $|S|$ decreases monotonically with V_g in all a- SnO_2 TTFTs due to the increase in n_s . It should be noted that the absolute value of S increased with decreasing SnO_2 thickness, showing the reduction of n_s . Since $-S$ values reflect the volume carrier concentration, we can estimate the effective electron channel thickness (t_{eff}) as $t_{\text{eff}} \equiv n_s/n_{3D}$, where n_{3D} is three-dimensional carrier concentration obtained from S - n_{3D} relationship as shown in Fig. S5.

Here we show the t_{eff} of the a- SnO_2 TTFTs during V_g application [Figs. 6(a)–6(d)]. t_{eff} gradually increased with V_g in all cases. The 6.2-nm-thick, 5.2-nm-thick, and 4.5-nm-thick SnO_2 TTFTs showed continuous increasing tendency of t_{eff} instead of reaching a saturation. This behavior is due to the high n_s along with the small regions of S modulation. And the maximum t_{eff} decreases as the thickness of the a- SnO_2 channel decreases. On the other hand, the 4.2-nm-thick SnO_2 TTFT showed clear saturation of t_{eff} (~ 1.4 nm) when $V_g > -6$ V. In other words, the depletion layer thickness is ~ 2.8 nm due to the oxygen adsorption, which agrees well with the previously reported depletion layer thickness.^{9, 15} From these results, we concluded that the optimal thickness of a-

SnO₂ is 4.2 nm for good TTFT showing rather large μ_{FE} ($\sim 20 \text{ cm}^2 \text{ V}^{-1} \text{ s}^{-1}$) and on-to-off current ratio ($\sim 10^5$).

We showed that the optimal thickness of a-SnO₂ for TTFT is 4.2 nm in the case of bottom-gate top-contact structure without a passivation layer. These results provide a guideline for realizing practical a-SnO₂ based TTFT. However, due to the strong gas-sensitive characteristics of SnO₂, the bottom-gate top-contact structure of the SnO₂ TTFT is ambiently unstable. Hence, further improvement is required such as use of a passivation layer on the top surface of SnO₂ layer or change the structure of the bottom-gate top-contact to enhance its ambient stability. We believe that the thickness of a-SnO₂ for TTFT with any gate structure can be optimized by analyzing the operation mechanism of the TTFTs using electric field thermopower modulation.

CONCLUSION

In summary, we have shown the optimization of SnO₂ film thickness for bottom-gate TTFTs. We systematically investigated the electron transport properties and the bandgap of SnO₂ films with various thickness. When the film thickness is thinner than 8 nm, the film becomes amorphous. The optical bandgap, carrier concentration, and Hall mobility of the 4-nm-thick amorphous SnO₂ film were $\sim 4.2 \text{ eV}$, $5 \times 10^{19} \text{ cm}^{-3}$, and

$\sim 15 \text{ cm}^2 \text{ V}^{-1} \text{ s}^{-1}$. Then, we optimized the SnO_2 thickness by analyzing the operation mechanism of the TTFTs using electric field thermopower modulation technique. As a result, TTFT based on the 4.2-nm-thick SnO_2 film exhibited excellent characteristics; highest on-to-off current ratio ($\sim 10^5$) and high mobility ($\sim 20 \text{ cm}^2 \text{ V}^{-1} \text{ s}^{-1}$). The present results would be essential to develop a- SnO_2 -based TTFTs in commercial applications.

EXPERIMENTAL PROCEDURES

Fabrication and Analyses of the SnO_2 thin films. SnO_2 films with different thicknesses were fabricated on SiO_2 glass substrates by pulsed laser deposition (PLD) technique (KrF excimer laser, $\lambda = 248 \text{ nm}$, fluence $\sim 0.3 \text{ J cm}^{-2} \text{ pulse}^{-1}$, repetition rate = 5 Hz) at a substrate temperature of 300 °C. After the film growth, the films were annealed at 400 °C for 30 min in air. The resultant films were analyzed by X-ray diffraction (XRD, $\text{Cu K}\alpha_1$, $\lambda = 1.54059 \text{ \AA}$, ATX-G, Rigaku Co.) measurements. Optical transmission and reflection spectra of the resultant films were measured using an ultraviolet-visible-near-infrared spectrometer (UV-vis-NIR, SolidSpec-3700, Shimadzu Co.) at RT. Electrical resistivity (ρ), carrier concentration (n), and Hall mobility (μ_{Hall}) of the SnO_2 thin films were measured by dc four-probe method with van der Pauw electrode configuration. Thermopower (S) was measured at RT.

Fabrication of the TTFTs. The bottom-gate top-contact TTFTs were fabricated as previous report.⁹ A 160-nm-thick polycrystalline HfO₂ film, which was deposited at room temperature, was used as the gate insulator film (the dielectric permittivity, $\epsilon_r = 21-23$ ¹⁶).

Thermopower analyses of the TTFTs. S of the TTFT channel was measured by conventional steady state method. Details of the electric field modulated S measurement are described elsewhere.¹⁷⁻²⁰

ASSOCIATED CONTENT

Supporting Information

Supporting Information is available free of charge via the Internet at <https://pubs.acs.org/doi/10.1021/acsaelm.xxxxxxx>.

$I_d^{0.5}-V_g$ curves of the bottom-gate top-contact a-SnO₂ TTFTs; Changes in the sheet carrier concentration (n_s) as function of V_g ; Changes in the field effect mobility (μ_{FE}) as function of V_g ; Optical absorption spectrum of the polycrystalline HfO₂ thin film deposited on SiO₂ glass substrate; Three-dimensional carrier concentration (n_{3D}) dependence S of the SnO₂ films.

AUTHOR INFORMATION

Corresponding Authors

Dou-dou Liang

The Beijing Municipal Key Laboratory of New Energy Materials and Technologies,

School of Materials Science and Engineering, University of Science and Technology

Beijing, Beijing 100083, China

ORCID: orcid.org/0000-0002-4112-2069

Email: liangdoudou1993@foxmail.com

Hiromichi Ohta

Research Institute for Electronic Science, Hokkaido University, N20W10, Kita,

Sapporo 001-0020, Japan

ORCID: orcid.org/0000-0001-7013-0343

Email: hiromichi.ohta@es.hokudai.ac.jp

Authors

Binjie Chen

Graduate School of Information Science and Technology, Hokkaido University,

N14W9, Kita, Sapporo 060-0814, Japan

ORCID: orcid.org/0000-0003-1838-2804

Hai Jun Cho

Research Institute for Electronic Science, Hokkaido University, N20W10, Kita,

Sapporo 001-0020, Japan

ORCID: orcid.org/0000-0002-8642-4183

Complete contact information is available at:

<https://pubs.acs.org/doi/10.1021/acsaelm.xxxxxxx>.

Author Contributions

D.L. and B.C. performed the sample preparation and measurements. D.L. and H.O. planned and supervised the project. All authors discussed the results and commented on the manuscript.

Funding Sources

Dou-dou Liang received scholarship from the China Scholarship Council (201806460051). Binjie Chen received scholarship from Japanese Government (Monbukagakusho: MEXT) Scholarship (191555). Hai Jun Cho received funding from Nippon Sheet Glass Foundation for Materials Science and Engineering. Hiromichi Ohta received founding from Grants-in-Aid of the JSPS (19H05791 and 17H01314).

Notes

The authors declare no competing financial interest.

ACKNOWLEDGEMENTS

This research was supported by Grants-in-Aid for Innovative Areas (19H05791) and Scientific Research A (17H01314) from the JSPS. D.L. greatly appreciates the support from China Scholarship Council (201806460051). B.C. appreciates the support from Japanese Government (Monbukagakusho: MEXT) Scholarship (191555). H.J.C. acknowledges the support from Nippon Sheet Glass Foundation for Materials Science and Engineering. A part of this work was also supported by Dynamic Alliance for Open Innovation Bridging Human, Environment, and Materials, and by the Network Joint Research Center for Materials and Devices.

REFERENCES

- (1) Nomura, K.; Ohta, H.; Takagi, A.; Kamiya, T.; Hirano, M.; Hosono, H., Room-temperature Fabrication of Transparent Flexible Thin-film Transistors using Amorphous Oxide Semiconductors. *Nature* **2004**, *432*, 488-492.
- (2) Nomura, K.; Takagi, A.; Kamiya, T.; Ohta, H.; Hirano, M.; Hosono, H., Amorphous Oxide Semiconductors for High-performance Flexible Thin-film Transistors. *Jpn. J. Appl. Phys.* **2006**, *45*, 4303-4308.
- (3) Kamiya, T.; Hosono, H., Material Characteristics and Applications of Transparent Amorphous Oxide Semiconductors. *NPG Asia Mater.* **2010**, *2*, 15-22.
- (4) Hosono, H., How We Made the IGZO Transistor. *Nat. Electron.* **2018**, *1*, 428-428.
- (5) Dattoli, E. N.; Wan, Q.; Guo, W.; Chen, Y. B.; Pan, X. Q.; Lu, W., Fully Transparent Thin-film Transistor Devices based on SnO₂ Nanowires. *Nano Lett.* **2007**, *7*, 2463-2469.
- (6) Sun, J.; Lu, A. X.; Wang, L. P.; Hu, Y.; Wan, Q., High-mobility Transparent Thin-film Transistors with an Sb-doped SnO₂ Nanocrystal Channel Fabricated at Room Temperature. *Nanotechnology* **2009**, *20*, 335204.
- (7) Huang, G.; Duan, L.; Dong, G.; Zhang, D.; Qiu, Y., High-mobility solution-processed tin oxide thin-film transistors with high- κ alumina dielectric working in enhancement mode. *ACS applied materials & interfaces* **2014**, *6*, 20786-20794.
- (8) Shin, C. W.; Chin, A.; Lu, C. F.; Su, W. F., Remarkably High Mobility Ultra-thin-film Metal-oxide Transistor with Strongly Overlapped Orbitals. *Sci. Rep.* **2016**, *6*, 19023.
- (9) Liang, D.-d.; Zhang, Y.-q.; Cho, H. J.; Ohta, H., Electric field thermopower modulation analyses of the operation mechanism of transparent amorphous SnO₂ thin-film transistor. *Appl. Phys. Lett.* **2020**, *116*, 143503.
- (10) Nagasawa, M.; Shionoya, S., Urbach's rule exhibited in SnO₂. *Solid State*

Communications **1969**, 7, 1731-1733.

(11) Lin, Y. H.; Faber, H.; Labram, J. G.; Stratakis, E.; Sygellou, L.; Kymakis, E.; Hastas, N. A.; Li, R.; Zhao, K.; Amassian, A., High Electron mobility thin-film transistors based on solution-processed semiconducting metal oxide heterojunctions and quasi-superlattices. *Advanced Science* **2015**, 2, 1500058.

(12) Chen, R.; Wang, W.; Lu, M.; Chen, Y.; Lin, H.; Chen, K.; Chen, L., Anomalous quantum efficiency for photoconduction and its power dependence in metal oxide semiconductor nanowires. *Nanoscale* **2013**, 5, 6867-6873.

(13) Sellers, M. C.; Seebauer, E. G., Manipulation of polycrystalline TiO₂ carrier concentration via electrically active native defects. *Journal of Vacuum Science & Technology A: Vacuum, Surfaces, and Films* **2011**, 29, 061503.

(14) Barlaz, D. E.; Seebauer, E. G., Manipulation of carrier concentration, crystallite size and density in polycrystalline anatase TiO₂ via amorphous-phase medium range atomic order. *CrystEngComm* **2015**, 17, 2101-2109.

(15) Lantto, V.; Rantala, T. T.; Rantala, T. S., Atomistic Understanding of Semiconductor Gas Sensors. *J. Eur. Ceram. Soc.* **2001**, 21, 1961-1965.

(16) Lin, Y.-S.; Puthenkovilakam, R.; Chang, J., Dielectric property and thermal stability of HfO₂ on silicon. *Applied physics letters* **2002**, 81, 2041-2043.

(17) Ohta, H.; Masuoka, Y.; Asahi, R.; Kato, T.; Ikuhara, Y.; Nomura, K.; Hosono, H., Field-modulated Thermopower in SrTiO₃-based Field-effect Transistors with Amorphous 12CaO-7Al₂O₃ Glass Gate Insulator. *Appl. Phys. Lett.* **2009**, 95, 113505.

(18) Ohta, H.; Mizuno, T.; Zheng, S. J.; Kato, T.; Ikuhara, Y.; Abe, K.; Kumomi, H.; Nomura, K.; Hosono, H., Unusually Large Enhancement of Thermopower in an Electric Field Induced Two-dimensional Electron Gas. *Adv. Mater.* **2012**, 24, 740-744.

(19) Sanchela, A. V.; Onozato, T.; Feng, B.; Ikuhara, Y.; Ohta, H., Thermopower

modulation clarification of the intrinsic effective mass in transparent oxide semiconductor BaSnO₃. *Phys. Rev. Materials* **2017**, *1*, 034603.

(20) Sanchela, A. V.; Wei, M.; Cho, H. J.; Ohta, H., Thermopower Modulation Clarification of the Operating Mechanism in Wide Bandgap BaSnO₃-SrSnO₃ Solid-Solution Based Thin Film Transistors. *Small* **2019**, *15*, 1805394.

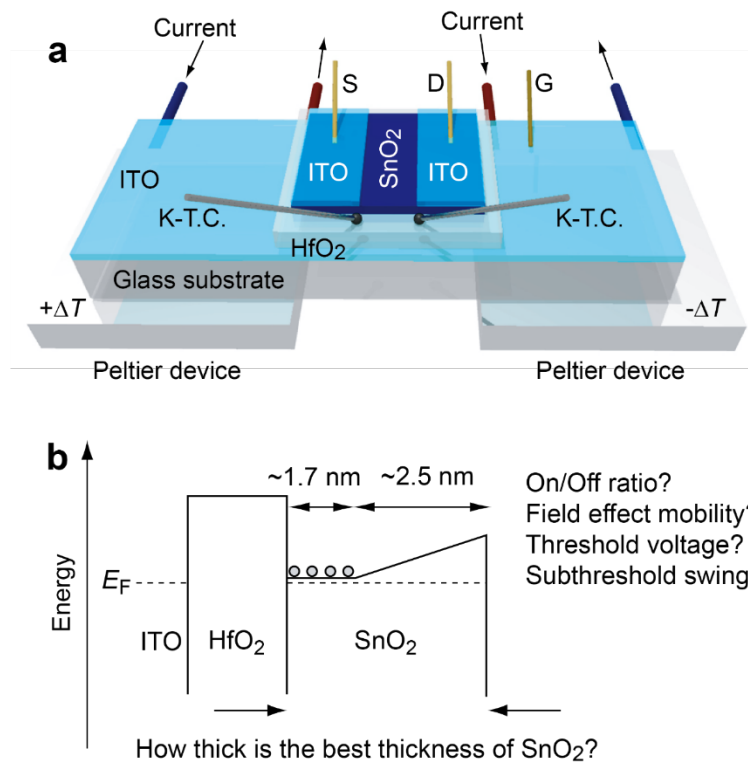


Figure 1. Concept of this research. (a) Schematic illustration of the electric field thermopower modulation measurement of the bottom-gate top-contact a-SnO₂ TTFT. (b) The energy band diagram around the conduction band of a-SnO₂ TTFT. Raised questions are the best thickness of SnO₂, on-to-off current ratio, field effect mobility, threshold voltage, and subthreshold swing.

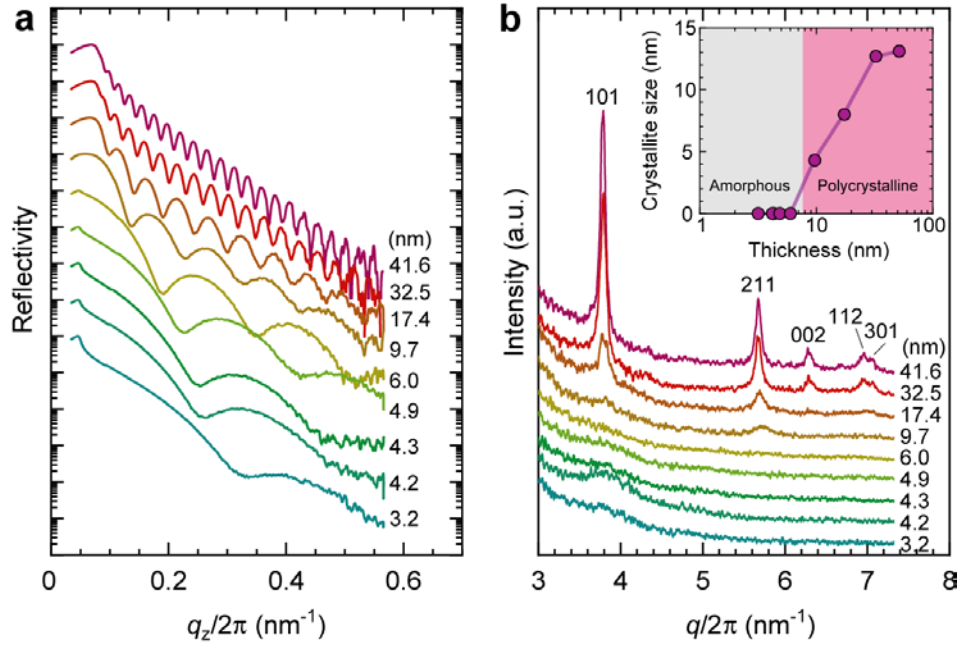


Figure 2. X-ray analyses of the SnO_2 thin films. (a) X-ray reflectivity of the SnO_2 thin films. The film thickness was calculated from the Kiessig fringes. (b) Glancing angle (0.5°) incidence X-ray diffraction pattern. The inset shows the crystallite size of the SnO_2 thin films, which was calculated from the diffraction peak of 211 using the Scherrer equation. When the thickness is thinner than 6 nm, the diffraction peak is not seen, indicating amorphous.

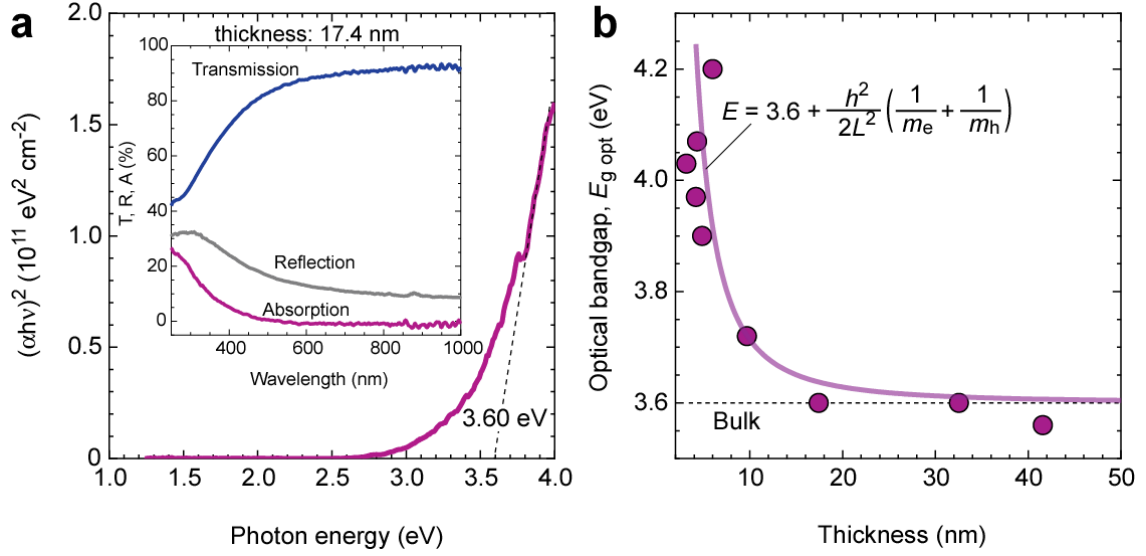


Figure 3. Quantum size effect of the SnO₂ thin films. (a) Tauc plot of the 17.4 nm-thick SnO₂ thin film deposited on SiO₂ glass substrate. The optical bandgap is 3.6 eV. Inset shows the transmission (*T*), reflection (*R*), and absorption (*A*) spectra. (b) Thickness dependent optical bandgap ($E_{g \text{ opt}}$). Dotted line shows bulk SnO₂ (3.6 eV). The $E_{g \text{ opt}}$ dramatically increases with decreasing thickness when the thickness is thinner than 10 nm, whereas thicker films (>18 nm) show bulk-like $E_{g \text{ opt}}$. The solid lines illustrate the calculated $E_{g \text{ opt}}$ for an infinite quantum well using Equation:

$$E_{g \text{ opt}} = 3.6 + \frac{h^2}{2L^2} \left(\frac{1}{m_e} + \frac{1}{m_h} \right).$$

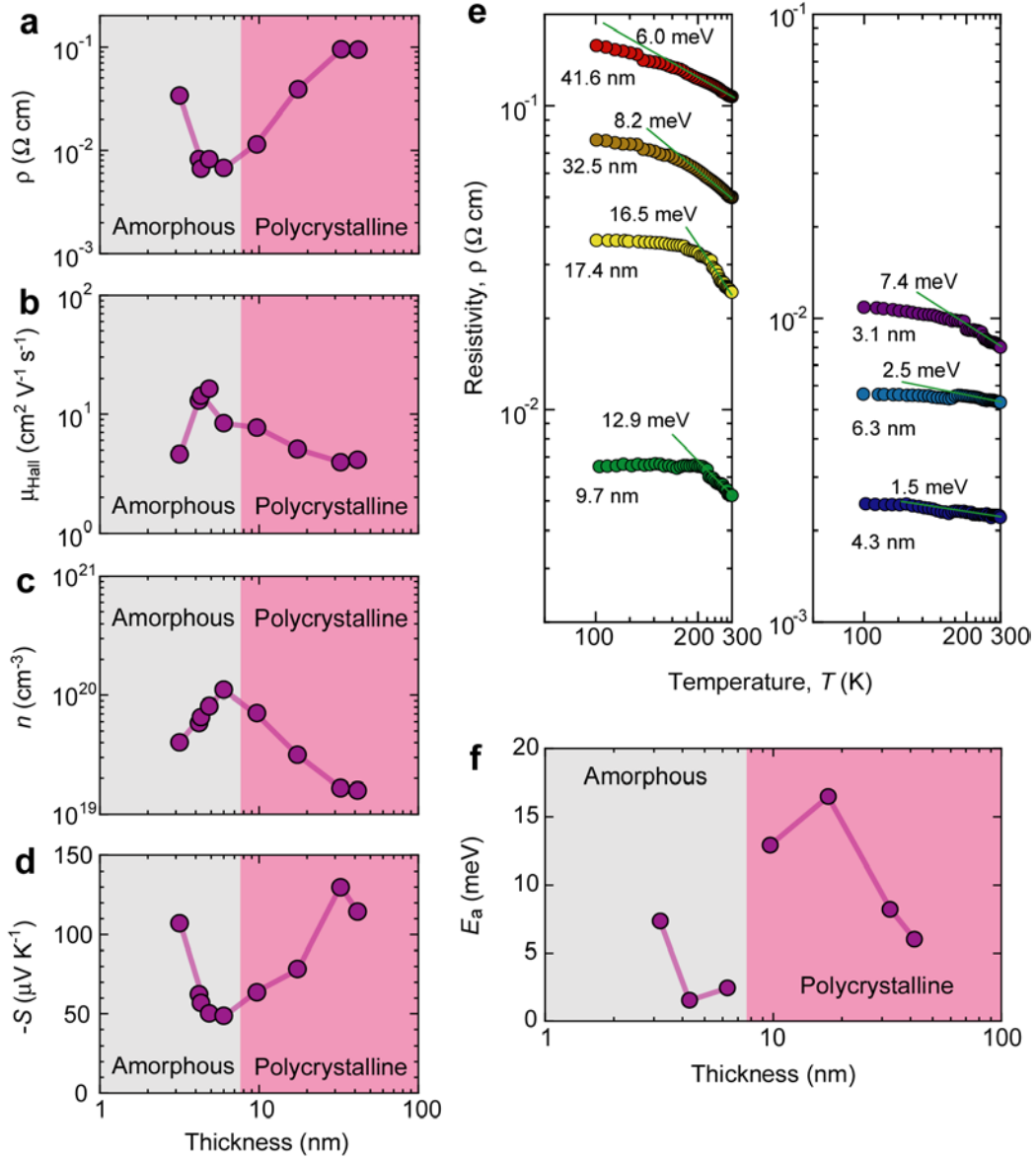


Figure 4. Electron transport properties of the SnO₂ thin films. Change in (a) resistivity (ρ), (b) Hall mobility (μ_{Hall}), (c) carrier concentration (n), (d) thermopower (S) as a function of the thickness of SnO₂ thin films. Note that the amorphous films showed opposite tendencies to the polycrystalline films. (e) Arrhenius plots of the ρ - T curves of the SnO₂ films. (f) The activation energy of the electrical conductivity (E_a), which was calculated from Fig. 4(e).

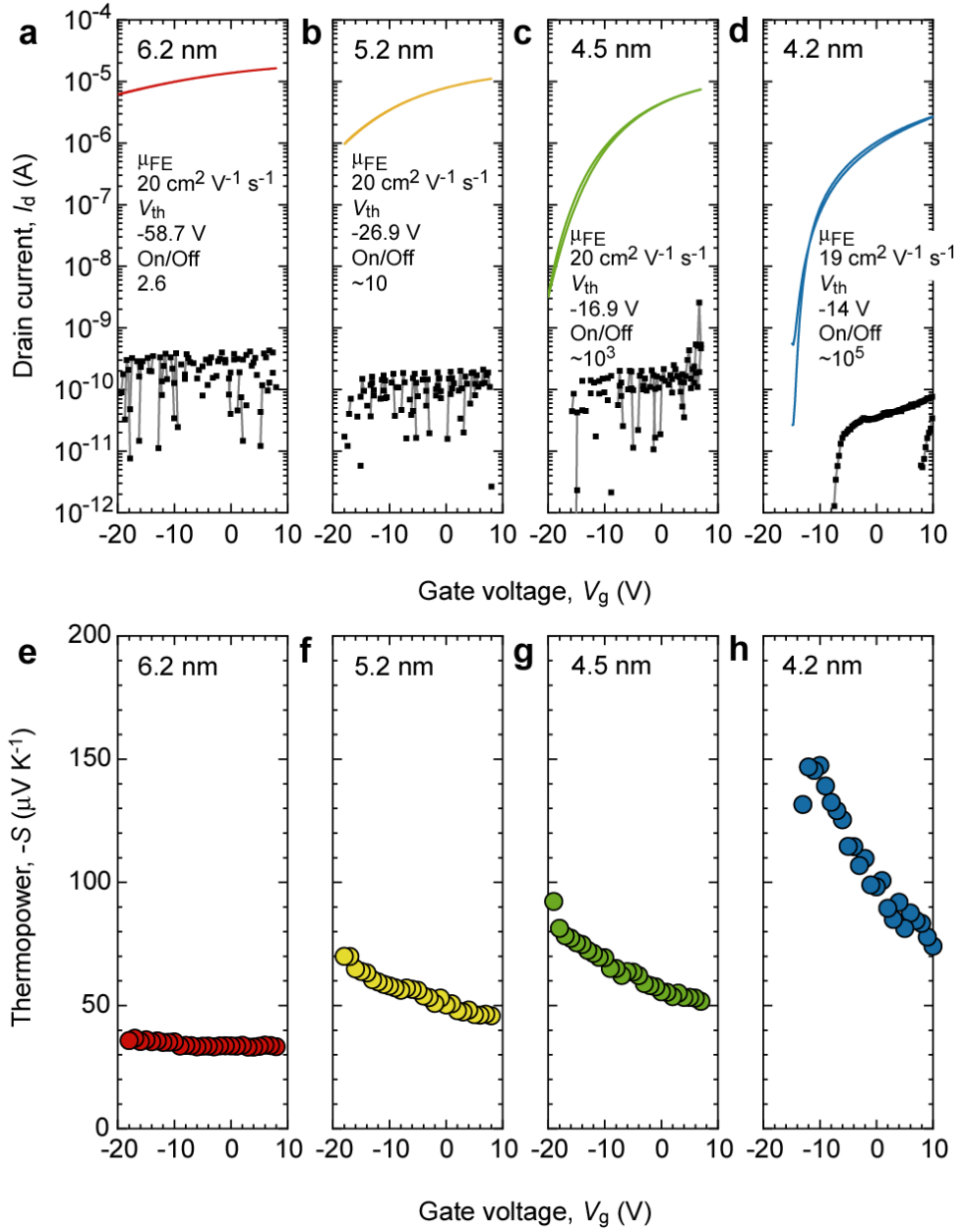


Figure 5. Electric field thermopower modulation analyses of the bottom-gate top-contact a-SnO₂ TTFTs. (a–d) Transfer (I_d – V_g) characteristics at $V_d = +0.1 \text{ V}$. Corresponding I_g – V_g curves are also shown (black square). The I_g is $< 300 \text{ pA}$. (e–h) Electric field modulated thermopower (S) at various V_g ranging from -20 V to $+8 \text{ V}$. The $-S$ gradually decreases with V_g .

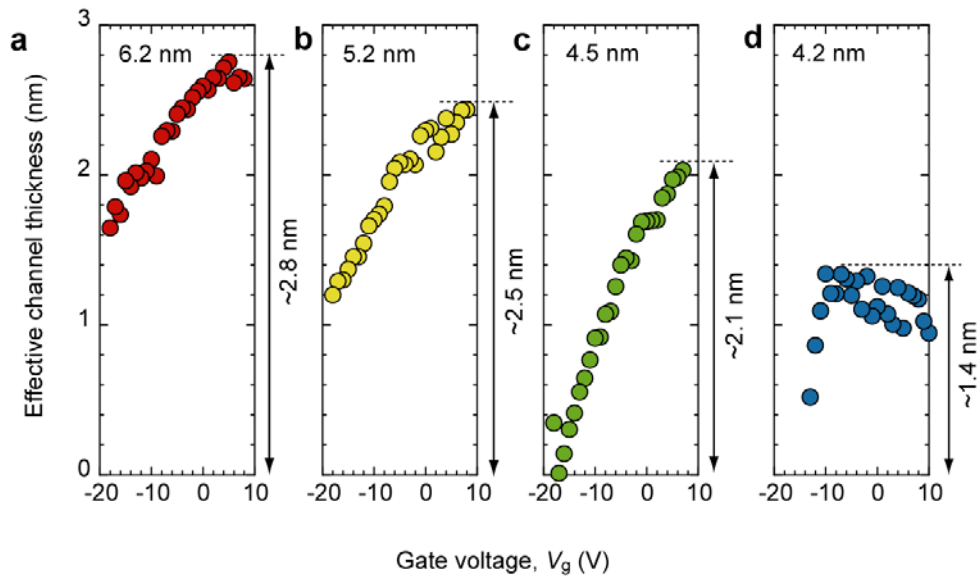


Figure 6. Effective channel thickness. (a–d) V_g dependence of the effective channel thickness (t_{eff}), which is defined as n_s/n_{3D} , decreases with decreasing the SnO₂ film thickness.

Supporting Information

Thickness Optimization toward High-Performance Bottom-Gated Transparent Tin Dioxide Thin-Film Transistor

Dou-dou Liang,^{*,1,2} Binjie Chen,³ Hai Jun Cho,^{2,3} and Hiromichi Ohta^{*,2,3}

¹The Beijing Municipal Key Laboratory of New Energy Materials and Technologies,
School of Materials Science and Engineering, University of Science and Technology
Beijing, Beijing 100083, China

²Research Institute for Electronic Science, Hokkaido University, N20W10, Kita,
Sapporo 001-0020, Japan

³Graduate School of Information Science and Technology, Hokkaido University,
N14W9, Kita, Sapporo 060-0814, Japan

*To whom correspondence should be addressed Email:

liangdoudou1993@foxmail.com, hiromichi.ohta@es.hokudai.ac.jp

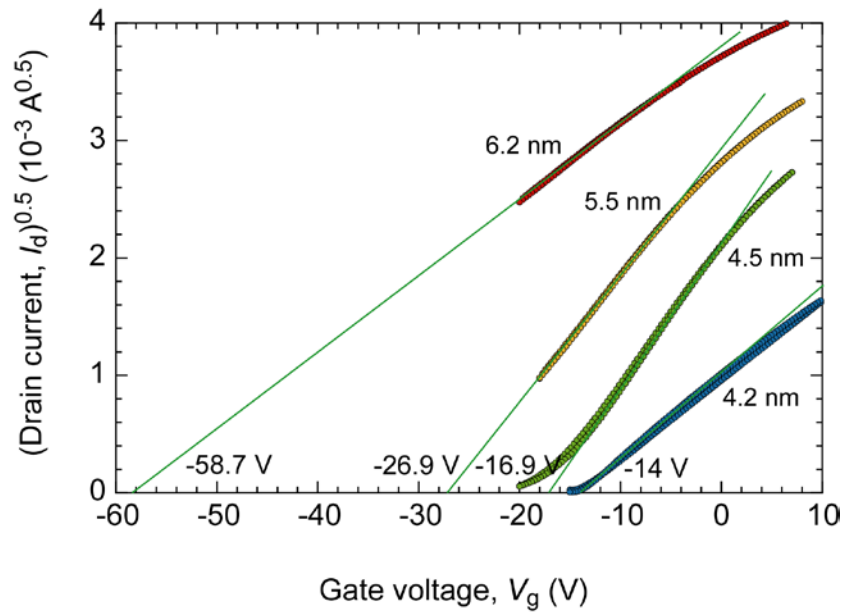


Figure S1. $I_d^{0.5}$ - V_g curves of the bottom-gate top-contact a-SnO₂ TFTs. The threshold voltage (V_{th}) is gradually decreasing with increased SnO₂ channel thickness.

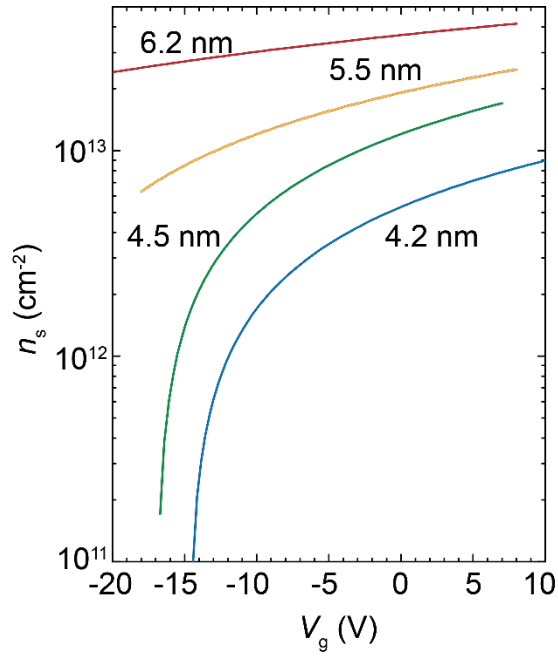


Figure S2. Changes in the sheet carrier concentration (n_s) as function of V_g . The sheet carrier concentration as the function of gate voltage (V_g) which was calculated by this formula [$n_s = C_i \cdot (V_g - V_{th}) \cdot e^{-1}$ where C_i is the capacitance per unit area ($C_i \sim 110 \text{ nF cm}^{-2}$) was measured using LCR meter and V_{th} is the threshold gate voltage that we can evaluate by plotting $I_d^{0.5} - V_g$ relationship].

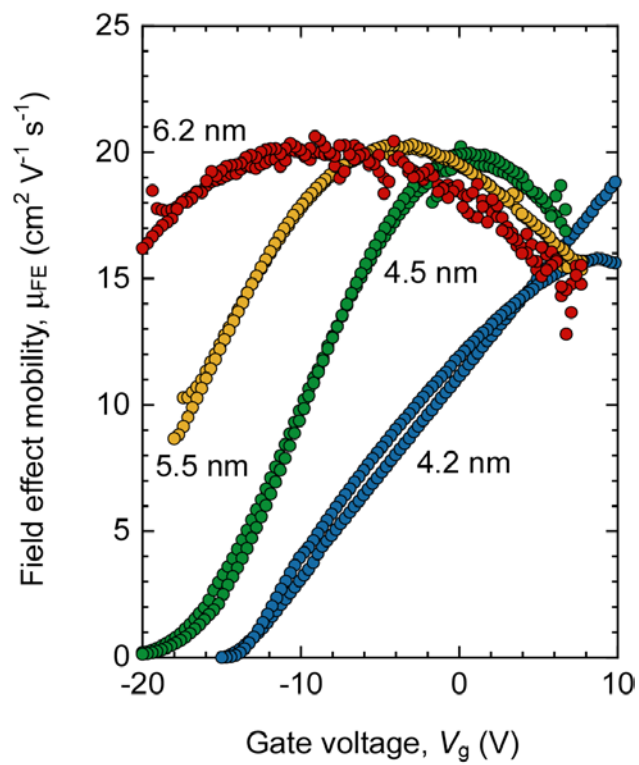


Figure S3. Changes in the field effect mobility (μ_{FE}) as function of V_g . The μ_{FE} reaches $\sim 20 \text{ cm}^2 \text{V}^{-1} \text{s}^{-1}$.

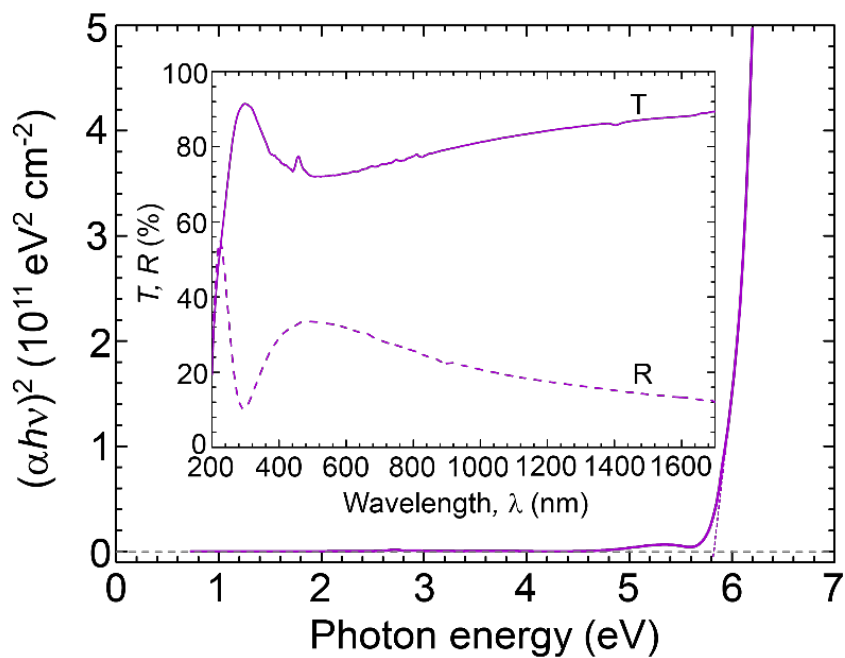


Figure S4. Optical absorption spectrum of the polycrystalline HfO₂ thin film deposited on SiO₂ glass substrate. The optical bandgap is 5.8 eV. Inset shows transmission (T) and reflection (R) spectra. Note the thickness of the HfO₂ film was 63.4 nm and the HfO₂ film was electrically insulator.

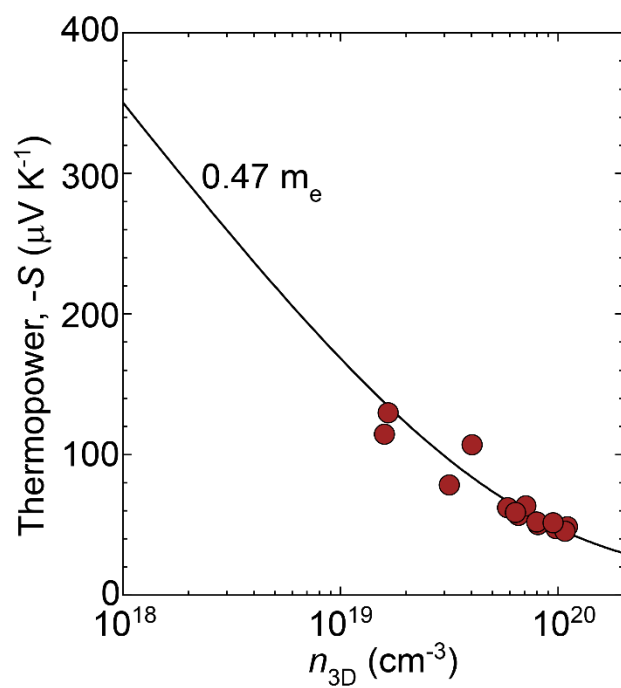


Figure S5. Three-dimensional carrier concentration (n_{3D}) dependence S of the SnO₂ films. The carrier effective mass (m^*) of the SnO₂ film around $0.47 m_e$.